ELECTROCHEMICAL STUDY OF TAYLOR–COUETTE FLOW BY LIMITING DIFFUSION CURRENT METHOD

Václav SOBOLÍK

Institute of Chemical Process Fundamentals, Academy of Sciences of the Czech Republic, 165 02 Prague 6, Czech Republic; e-mail: sobolik@icpf.cas.cz

Received April 21, 1998
Accepted December 23, 1998

Steady Taylor vortices were studied by electrodiffusion probes in the gap between coaxial cylinders. The inner cylinder was driven by a stepping motor and the outer cylinder was fixed. The viscosity of standard potassium hexacyanoferrates (III) and (IV) aqueous solution was increased to 2.52 mPa s by addition of poly(alkylene glycol) Emkarox 45. The velocity gradient components were measured by two three-segment probes at the wall of the outer cylinder for four radius ratios, R_1/R_2 = 0.8, 0.75, 0.65 and 0.6. The axial distribution of the azimuthal and axial components of velocity gradient was mapped while Taylor vortices were swept along the probes by a slow axial flow. The components of velocity gradient were described by fourth-order Fourier series. Generalized dependencies were found of the Fourier coefficients on Taylor number. A vertical shift of the probes made it possible to calculate the wavelength and the drifting velocity of Taylor vortices. Critical Taylor numbers were estimated from the axial component of velocity gradient and by the flow visualization using a rheoscopic liquid. The torque was calculated from the azimuthal component of velocity gradient.

Key words: Electrodiffusion method; Three-segment probes; Taylor vortices; Electrochemistry.

Due to the centrifugal forces the laminar flow in the gap between an inner rotating and outer fixed coaxial cylinders becomes unstable at a critical Taylor number. Toroidal counter-rotating Taylor vortices with a height equal approximately to the gap width replace the original Couette flow[1]. At higher rotation rates, azimuthal waves are superposed on the Taylor vortices. Further increase in rotation rate induces azimuthal waves with modulated amplitude, then turbulent flow occurs in cells occupied earlier by vortices and, finally, the turbulent flow spreads throughout the whole gap. Taylor vortices and the following states have been studied both theoretically[2] and experimentally[3].

Taylor–Couette flow with a superposed slow axial flow has many potential applications. Legrand and Coeuret[4] and Desmet *et al.*[5] studied mixing in cells with the aim of making use of this type of flow in chemical reactors

because the time distribution spectrum is very narrow and the velocity gradients are low. Kataoka *et al.*[6] showed that flow with modulated azimuthal waves and weakly turbulent cells is convenient for emulsion polymerization of styrene. Taylor vortices are used for the prevention of concentration polarization and membrane fouling in separation processes[7].

Wall velocity gradient or wall shear stress is an important parameter in the above applications. Their mean values are known from torque measurements[8]. However, these measurements do not elucidate the gradient distribution. The gradient maximum could be much greater than the mean values. Cognet[9] measured the maximum and minimum values of the limiting diffusion current on the wall of the outer fixed cylinder in Taylor–Couette flow. He used a simple circular electrode and did not interpret the results as a wall velocity gradient. Sobolík *et al.*[10] showed that three-segment electrodiffusion probes are capable of mapping the azimuthal and axial components of the wall velocity gradient.

This study is devoted to systematic measurements of velocity gradients at the outer wall of a cylindrical Couette apparatus with stable Taylor vortices. The axial distribution of the azimuthal and axial components is studied as a function of rotation rate and inner cylinder diameter. Three-segment electrodiffusion probes are used for the decomposition of wall velocity gradient into its components. This paper is an extension of the previous paper[10] in the following directions. Two vertically shifted probes are used to verify the measurements and to obtain the axial scale – wavelength of vortices. The diameter ratio of the cylinders is extended to 0.65 and 0.6. A more viscous fluid is used to get a better accuracy, especially near critical Taylor numbers for small η. A better control of the inner cylinder rotation is achieved by using a stepping motor.

EXPERIMENTAL

Experimental Apparatus

The experimental apparatus is shown in Fig. 1. It consisted of an outer cylinder 3 made of a Plexiglas tube with an inner diameter of $R_2 = 60.7 \pm 0.2$ mm and an interchangeable inner Plexiglas cylinder 4. The inner cylinders had a length of 275 mm and diameters of R_1 = 48.5, 45.5, 39.4 and 36.4 mm. For calibration of electrodiffusion probes *in situ*, annular rings with an outer diameter of 57.6 mm could be slid on each cylinder. Higher velocity gradients in a still laminar Couette flow were achieved in this small gap of 1.55 mm. The corresponding radius ratios, $\eta = R_1/R_2$, were 0.95, 0.8, 0.75, 0.65 and 0.6. The inner cylinder was mounted on the stainless steal shaft 5 which had an upper ball bearing and bottom polyamide sliding bearing. The shaft was driven by a stepping motor with a step of 0.9° and a gear box with a slow-down ratio of 1 : 9. There was a plastic clutch between the shaft and gear box which

also served as electrical insulation. The revolutions were controlled by a computer directly from the measuring software.

Two three-segment electrodiffusion probes 1 and 2 were embedded in the wall of the outer cylinder. The probes faced each other, which meant that the angle between them was 180°, but they were not at the same horizontal level. The vertical shift of 5 mm enabled calculation of the length of vortices from the measured signals. With the aim of obtaining the axial distribution of the velocity gradient components, the Taylor vortices were swept along the probes by a small axial flow. The liquid was circulated by a pump (Fluid Metering Inc.) with a valveless piston head (RH0CKC) having a piston of a diameter of 1/16''. The maximum volume per stroke was 0.05 ml and the maximum flow rate was 0.38 ml s^{-1}. The test liquid was pumped from a small tank with a volume of one litre into an inlet tube in the bottom of the apparatus. An outlet tube was mounted 8 mm below the cover and connected to the tank by a hose. The temperature of the liquid in the tank was controlled by a cooling coil.

Limiting Diffusion Current Method

The measurement of wall velocity gradients by means of the limiting diffusion current is a well-known technique[11]. A two-electrode cell consisting of a small working electrode and a large auxiliary electrode, a solution containing depolarizer and excess supporting electrolyte is sufficient for measuring the limiting diffusion current. The applied voltage must have a

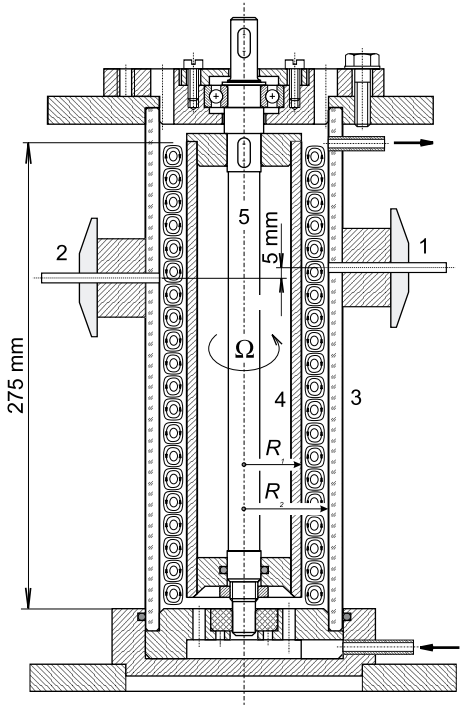

FIG. 1
Experimental set-up with Taylor vortices: 1, 2 three-segment electrodiffusion probes, 3 outer cylinder, 4 inner cylinder, 5 shaft

value at which only the active species react on the working electrode and their concentration on this electrode is negligibly small. If the Peclet number is sufficiently high, only the term of the molecular diffusion perpendicular to the electrode surface and convective terms stay in the mass transfer equation. The transport of species to the working electrode and thereby the electric current are then controlled only by the velocity field in the vicinity of the working electrode. The Schmidt numbers are above 1 000 in aqueous solutions of depolarizers and so the concentration boundary layer is much thinner than the momentum boundary layer. The velocity distribution in such a thin concentration boundary layer can be approximated by a linear profile of slope equal to the velocity gradient at the wall. The analogous problem of heat transfer was first solved by Leveque[12]. According to this solution, the current density is given by

$$i(x) = \frac{nFc_0 D^{2/3} \gamma^{1/3}}{9^{1/3} \Gamma(4/3) x^{1/3}} , \qquad (1)$$

where x is measured along a streamline from the front edge of the electrode. The current density and concentration boundary layer on the working electrode are shown in Fig. 2. The concentration of active species is negligibly small at the electrode surface and equals c_0 in the bulk. The shadows in Fig. 2 stand for concentration. The darker the shadow the smaller the concentration. The total current is calculated by integration of the current density over the whole electrode surface. For example, for a strip electrode with length L in the flow direction and width W,

$$I = 0.808 nFc_0 D^{2/3} W L^{2/3} \gamma^{1/3} . \qquad (2)$$

According to Eq. (*1*) the current density decreases with $x^{-1/3}$ and hence the total current depends on $L^{2/3}$. This fact makes it possible to evaluate the flow direction by using segmented probes composed of several electrically insulated parts. Three-segment probes are capable of

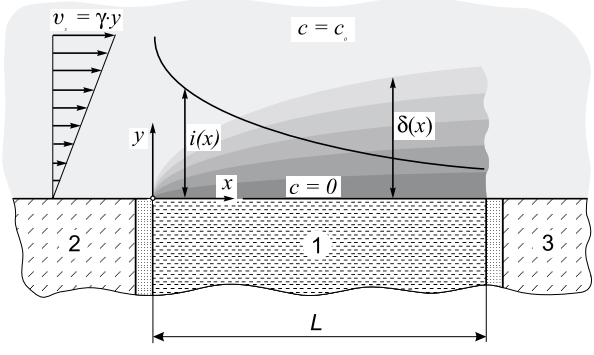

FIG. 2
Concentration boundary layer and current density on electrode: 1 working electrode, 2 wall, 3 auxiliary electrode

flow angle resolution in the whole interval of 360°. An ideal three-segment probe is shown in Fig. 3. Intensity of current density is denoted by shading. The darker the shading the higher the current density. If the velocity gradient is uniform, the ratios of currents through the segments depend only on the flow direction. The dependences of the limiting diffusion currents through segments, I_k, normalized by the sum of the currents, I_{tot}, on the flow direction are called directional characteristics. Directional characteristics of the ideal three-segment probe with negligibly thin insulating gaps, calculated by means of Eq. (*1*), are compared with the real directional characteristics of the probe 1 in Fig. 4. The microphotograph showing the surface of this probe is shown in Fig. 5. The real directional characteristics were measured *in situ* in the laminar Couette flow by turning the probe in steps of 15° relative to steady azimuthal flow. The characteristics were fitted by fourth-order Fourier series.

The amplitudes of real characteristics are smaller than those of the ideal probe. This is due to the finite insulation gaps between segments over which the solution concentration

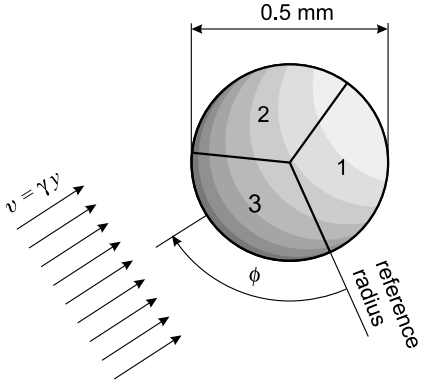

FIG. 3
Ideal three-segment probe in uniform flow

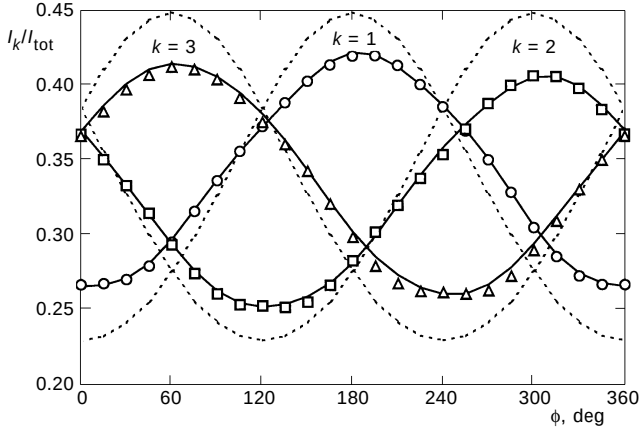

FIG. 4
Directional characteristics of probe 1: Δ segment *1*, ❍ segment *2*, ❐ segment *3*; full lines – fourth-order Fourier series, dotted lines – ideal probe

partially recovers. The first coefficient of the Fourier series, *i.e.* the mean value of the characteristic over the whole angle ϕ, is proportional to the segment area. It follows from Fig. 5 that the segment areas of the probe are slightly different. In experiments, the flow angle is evaluated on-line from the measured segment currents. The currents are normalized and compared. The flow angle is then calculated from the intermediate current because variation of this current is most sensitive to the flow angle. The accuracy of the flow angle measurement is better than 4°.

The condition of high Peclet number was not fulfilled in our experiments. Therefore the total current was not proportional to $\gamma^{1/3}$ and an empirical relation[10]

$$I_{\mathrm{tot}} = b_1\gamma^{1/3} + b_2\gamma^{-1/3} + b_3\gamma^{-1/6} \qquad (3)$$

was used. The coefficients in Eq. (*3*) were found by calibration *in situ* in Couette flow before each set of measurements.

The limiting diffusion current is revealed by a plateau on the polarogram (*I*–*U* dependence). The existence of the plateau is necessary for obtaining reliable results and the polarogram was therefore measured before each set of measurements. A voltage of –0.8 V was applied between the working electrodes (cathodes) and auxiliary electrode (anode).

A new method of making use of transient currents was recently described for calibration and verification of electrodiffusion systems[13]. Active electrode area, coefficient of diffusion or species concentration can be calculated from the transient current measured after application of polarization voltage step from the equilibrium value to a value corresponding to the limiting diffusion current. If the above mentioned parameters are constant, the measured Cottrell asymptote has also constant value. This method was used for verification of our electrodiffusion system during the measurements of Taylor vortices.

The three-segment probes were made in house. Three platinum wires with a diameter of 0.5 mm were pulled simultaneously through a wire-drawing die, starting with a diameter of 1 mm and finishing with 0.5 mm. After drawing, the wires took a cross-section shape shown in Fig. 5. The wires were then coated electrophoretically with a polymeric paint and glued together with Epoxy 1200 (United Chemical and Metallurgical Works, Ústí n. L., Czech Republic). After soldering the connecting cables, the wires were glued with Epoxy 521 (a product of the same company) into a stainless steel tube with a tip diameter of 3 mm. The tip was then ground with emery paper and finally polished with an emery paper with a grit size of 15 μm.

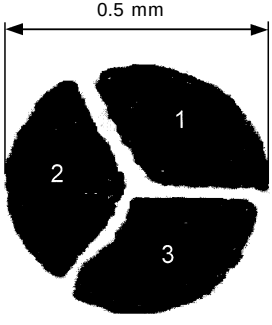

FIG. 5
Microphotograph of probe 1

To avoid electrical noise it was necessary to join all stainless steel parts of the Couette apparatus which are in contact with the electrolyte and to polarize them as counter electrode. Hence, the electrode tube was connected to the stainless steel shaft and the inlet and outlet tubes. A small piece of platinum sheet was put into the inlet tube.

The three-segment probes were connected to a six-channel electrodiffusion analyzer, which applied the polarization voltage to the electrodes and converted the currents flowing through the electrodes into voltages. The analyzer was controlled by a PC *via* an A/D and D/A card. The data were treated on-line to give velocity gradient components which were shown in a phase diagram on the screen.

The test liquid was a 25 mol m^{-3} equimolar potassium hexacyanoferrates (III) and (IV) aqueous solution (nF = 96 485 C mol^{-1}) with 1.5% b.w. K_2SO_4 as supporting electrolyte. The addition of 3% b.w. of poly(alkylene glycol) Emkarox 45 (ICI, Frankfurt, Germany) enhanced the dynamic viscosity of the resulting electrolyte to 2.52 mPa s at 23 °C. The density of the electrolyte was 1 024 kg m^{-3}. The flow was visualized by addition of a few drops of rheoscopic liquid AQ-1000 (Kalliroscope Corp., U.S.A.). The rheoscopic liquid contains small laminae reflecting light in dependence on their orientation which follows the flow direction.

Kinematics of Taylor Vortices

When the Taylor number reaches a critical value, laminar Couette flow is no longer stable and disturbances appear which ultimately take the form of cellular, toroidal vortices, regularly spaced along the axis z. The cylindrical coordinates, r, θ, z, the corresponding velocity components, v_r, v_θ, v_z, and a "stream tube" of a Taylor vortex are shown in Fig. 6. The ve-

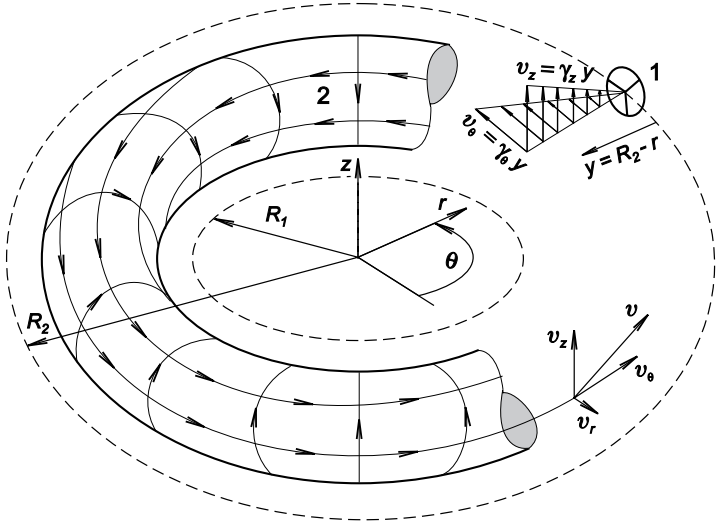

FIG. 6
Schematized flow situation: 1 probe, 2 Taylor vortex tube

locity field measured by probe 1 is shown in a magnified view. The velocity components of a steady vortex have axial symmetry (do not depend on θ) and are periodic functions of *z*:

$$\upsilon_r(r,z) = \sum_k \upsilon_{rk}(r)\cos[k\alpha z + \varphi_{rk}(r)] \tag{4}$$

$$\upsilon_\theta(r,z) = \overline{\upsilon_\theta}(r) + \sum_k \upsilon_{\theta k}(r)\cos[k\alpha z + \varphi_{\theta k}(r)] \tag{5}$$

$$\upsilon_z(r,z) = \sum_k \upsilon_{zk}(r)\sin[k\alpha z + \varphi_{zk}(r)]\,. \tag{6}$$

The phases φ_{ik} are always equal to 0 at the outer wall and can achieve values of 0 or π elsewhere. The origin of *z* is in the plane where υ_r exhibits its maximum, that is in the "stagnation line" of a jet impinging on the outer wall ($\gamma_\theta(z = 0) = \max$ and $\gamma_z(z = 0) = 0$).

Linear theory[14] predicts the critical Taylor number and wavenumber of the vortices. Nonlinear theories[15,16] take into account the distortion of the mean flow by disturbances and are capable of predicting the growth of velocity components with Taylor number. Critical Taylor numbers are given in a recent review[17]. The axial, υ_z, and radial, υ_r, velocity components are related by the equation of continuity, $\upsilon_r/r + \partial\upsilon_r/\partial r + \partial\upsilon_z/\partial z = 0$.

As the concentration boundary layer at the electrodiffusion probe is very thin, we can neglect the curvature of the wall and introduce a new coordinate $y = R_2 - r$, which represents normal distance from the wall. Only two components of the velocity gradient tensor have a nonzero value at the outer wall

$$\left.\frac{\partial\upsilon_\theta}{\partial y}\right|_{y=0} \equiv \gamma_\theta(z) = \gamma_m + \sum_k \gamma_{\theta k}\cos k\alpha z \tag{7}$$

$$\left.\frac{\partial\upsilon_z}{\partial y}\right|_{y=0} \equiv \gamma_z(z) = \sum_k \gamma_{zk}\sin k\alpha z\,. \tag{8}$$

The azimuthal, γ_θ, and axial, γ_z, components can be evaluated by the three-segment probes from the directional characteristics under the assumption that the normal velocity, υ_r, is negligible or, in other words, that the axial component does not depend strongly on *z* (ref.[18]).

The rate of deformation tensor is necessary for the calculation of the shear stress tensor. The components of the shear rate tensor at the wall are identical with the components of the velocity gradient tensor. Hence for the shear stress components on the outer wall ($r = R_2$) holds: $\tau_{r\theta}(z) = \mu\gamma_\theta(z)$, $\tau_{rz}(z) = \mu\gamma_z(z)$.

RESULTS AND DISCUSSION

The experiments were carried out as follows. The gap between the cylinders was filled with the solution up to the outlet tube and the pump was

stopped. The rotation rate was very slowly increased from a value corresponding to laminar Couette flow and γ_θ and γ_z were followed on the screen in a phase diagram and flow pattern in the gap was observed. When the first disturbance appeared, the revolutions were kept constant and it took several minutes until Taylor vortices were fully developed. The first disturbance manifested itself by a nonzero γ_z value and a fully developed stable vortex by constant values of γ_θ and γ_z. An axial upwards flow was then started. Taylor vortices were swept by this flow. The vortex at the bottom was stable whereas the next one elongated until it split periodically into two vortices. The movement of vortices along the probes was regular as shown in Fig. 7. There is a time history of γ_θ and γ_z of two pairs of vortices, measured by the two probes. The sampling frequency of the segment currents was 3 000 s^{-1}. Instantaneous values of γ_θ and γ_z were calculated on-line and their mean values and standard deviations were recorded every 0.9 s. For better distinction, only every third point is depicted in Fig. 7. By using two electrodiffusion probes, the measured velocity gradient components are verified immediately. The vertical shift of the probes makes it possible to calculate the wavelength and sweeping velocity of Taylor vortices. The time lag between signals is denoted by *s* and corresponds to the vertical distance of 5 mm between the probes, see Fig. 1. The wavelength can be then calculated from the period *T*. The periodicity of γ_θ and γ_z shown in Fig. 7 over two periods indicates that the subsequent moving Taylor vortices are

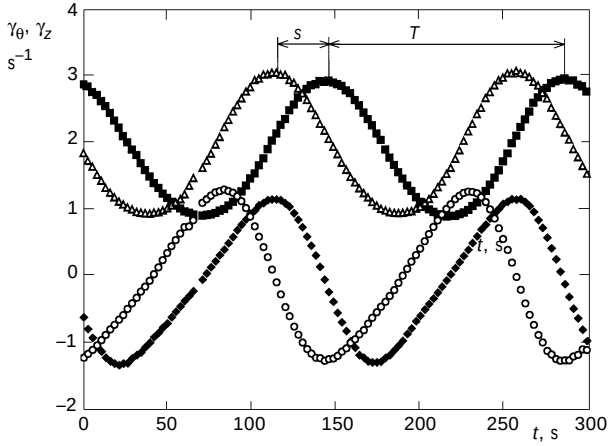

FIG. 7
History of velocity gradient components at $\eta = 0.65$ and $\Omega = 1.05$ rad s^{-1}. Probe 1: ■ γ_θ, ◆ γ_z; probe 2: Δ γ_θ, ❍ γ_z

identical. Relative deviations between corresponding amplitudes measured by two probes were smaller then 10%. These deviations were caused mostly by calibration errors due to non-circularity of the outer cylinder.

Critical Taylor numbers were estimated in three different ways. The first was by on-line measurement of γ_z, which is different from zero when a disturbance appears in the Couette flow. This component is also zero at the "stagnation lines" of a stable Taylor vortex, but during the transition the flow is not stable. The second method uses flow visualization with a rheoscopic liquid. The most precise way is to evaluate Ta_c as the intersection of the extrapolated measured dependences of the velocity gradient or its arbitrary component of the Coutte flow and the Taylor vortex flow. This method gives the best results which are very close to the values reviewed by Di Prima and Swinney[17] and will be elucidated later on. Measured critical rotation rates, velocity gradients and Taylor numbers are summarized in Table I. The dependence of Ta_c on η is shown in Fig. 8. In the interval $\eta \in \langle 0.5,1 \rangle$, the data[17] can be fitted using relation

$$Ta_c = 36.2\ (\eta - 0.256)^{-0.445}\ , \qquad (9)$$

which has a standard deviation of $\sigma = 0.24$.

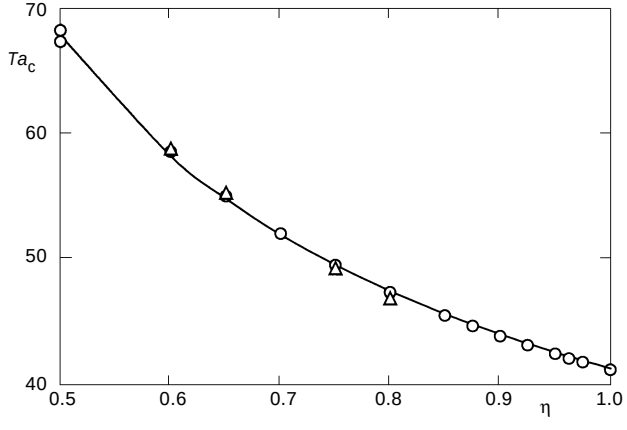

FIG. 8
Dependence of critical Taylor number on radius ratio: ❍ full line – least square fit of published data[17], Δ present measurements

In Fig. 9 the dependences of γ, γ_θ and γ_z on the z coordinate are depicted for the extreme values of rotation rate in all four gap widths. In the smallest gap, $\eta = 0.8$, not far above the Ta_c, the $\gamma(z)$, $\gamma_\theta(z)$ and $\gamma_z(z)$ have near-sinusoidal form, which can be described by the first harmonics and $\gamma_\theta(z)$ merges into $\gamma(z)$. The greater the gap and rotation rate the more harmonics are necessary and the greater are deviations between $\gamma(z)$ and $\gamma_\theta(z)$. The form of $\gamma_z(z)$ in Figs 9f and 9h resembles the wall velocity gradient distribution near the stagnation point of an impinging jet. Near the "stagnation lines", $\gamma_z(z) = 0$, $z = k\pi/\alpha$ ($k = 0, 1, ..., n$), where the change of γ_z with z is rather strong, the condition of uniform velocity gradient on the probe area is violated. The estimation of flow angle from the directional characteristics measured in viscometric flow is then not exact. The profiles of measured velocity gradient at $\gamma_z = 0$, especially that of $\gamma(z)$ and $\gamma_\theta(z)$, are slightly asymmetric. This asymmetry is smoothed by fitting the data by Fourier series. The amplitudes of the harmonics follow from Fig. 10 where they are shown as a function of rotation rate for all four measured geometries.

It is possible to generalize the dependences of the harmonics on rotation rate by dividing the harmonics by the critical velocity gradient of transition to Taylor vortex flow, γ_c, and Taylor number by its critical value (see Fig. 11). These dependences were fitted by second-order polynomials with results summarized in Table II.

Couette–Taylor flow has often been studied by torque measurements. The torque, G, can be calculated from the mean value of $\gamma_\theta(z)$, γ_m, on the outer cylinder. It is convenient to introduce the dimensionless torque G^* as the mean velocity gradient on the inner cylinder divided by the rotation rate.

TABLE I
Main experimental parameters, transition values, wavelengths of vortices and axial Reynolds numbers

η	R_1 mm	d mm	Ω_c rad s^{-1}	γ_c s^{-1}	Ta_c	T °C	$\nu \cdot 10^6$ m^2 s^{-1}	λ nm	Re_{ax}
0.80	24.25	6.05	1.560	5.55	46.9	23	2.46	13.7–14.7	0.29
0.75	22.75	7.55	1.211	3.11	49.3	24	2.39	16.3–17.5	0.45
0.65	19.70	10.60	0.911	1.33	55.3	23.3	2.44	20.8–24.3	1.11
0.60	18.20	12.10	0.806	0.91	58.8	23	2.46	24.1–28.9	1.14

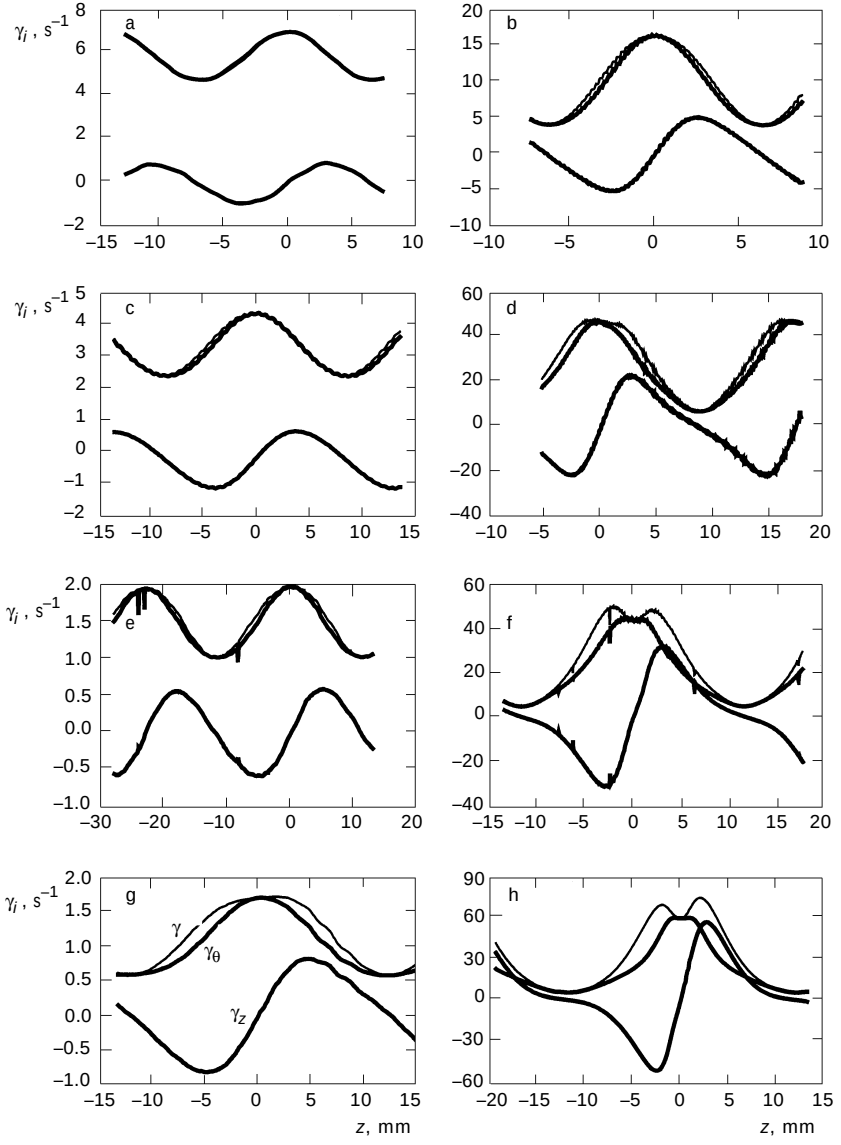

FIG. 9

Examples of γ, γ_θ and γ_z axial distribution: thick lines γ_θ and γ_z, thin line γ; η = 0.8: a Ω = 1.56 rad s^{-1}, b Ω = 1.97 rad s^{-1}; η = 0.75: c Ω = 1.2 rad s^{-1}, d Ω = 3.98 rad s^{-1}; η = 0.65: e Ω = 0.911 rad s^{-1}, f Ω = 5.24 rad s^{-1}; η = 0.6: g Ω = 0.942 rad s^{-1}, h Ω = 7.33 rad s^{-1}

$$G^* = \frac{G}{\Omega \mu R_1^2 L} = \frac{2\pi\gamma_m}{\eta^2 \Omega} \qquad (10)$$

G^* of the laminar Couette flow depends only on η, $G^* = 4\pi/(1 - \eta^2)$. The measured dependences of G^* on *Ta* are shown in Fig. 12. The critical Taylor number could be found as intersection of the extrapolated dependence $G^*(Ta)$ for Taylor vortex flow with Couette flow. It is obvious that for evaluation of G it is necessary to use a three-segment probe, because a simple probe gives only $\gamma(z)$, from which it is impossible to get a correct value of γ_m.

The dependence of the torque on Taylor number can be expressed as

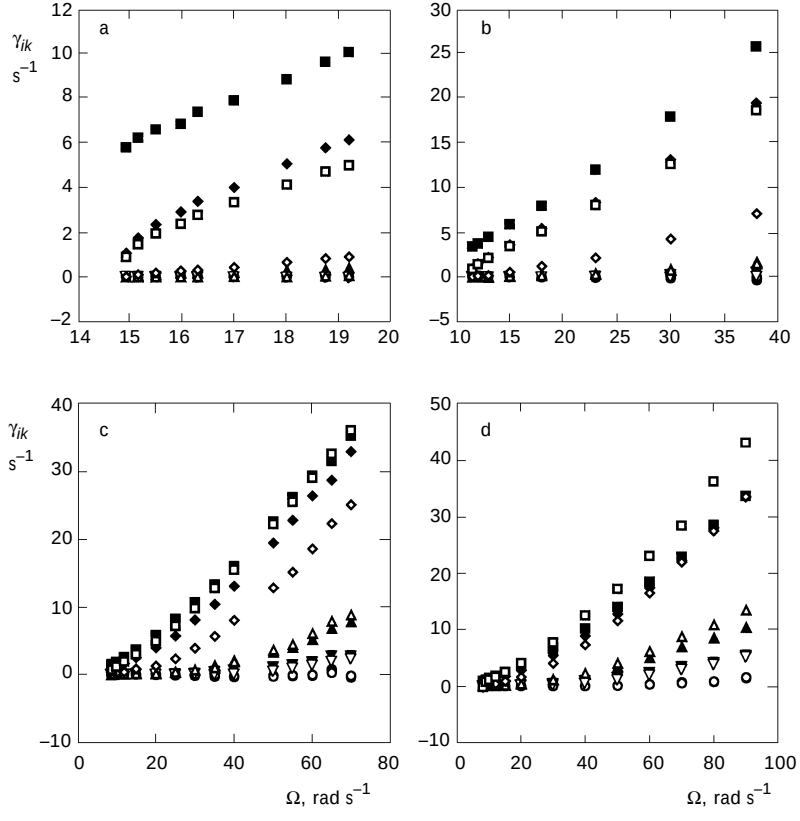

FIG. 10

Dependence of Fourier coefficients, Eqs (*7*) and (*8*), on η and Ω: a η = 0.8, b η = 0.75, c η = 0.65, d η = 0.6; ■ γ_m, ◆ $\gamma_{\theta 1}$, ▲ $\gamma_{\theta 2}$, ▼ $\gamma_{\theta 3}$, ● $\gamma_{\theta 4}$, ❒ γ_{z1}, ✧ γ_{z2}, Δ γ_{z3}, ∇ γ_{z4}, ❍ γ_{z5}

$$G^* = aTa^{-2} + bTa^{c} \quad . \tag{11}$$

Stuart[15] found the torque by an energy-balance method for the limiting case of a small gap, $\eta \to 1$. His result is expressed by Eq. (*11*) with $c = 0$. Davey[16] used a rigorous perturbation expansion for solving the velocity of Taylor vortices under the assumption that the amplitude is sufficiently small. According to Davey, the exponent c again equals zero, but the coefficients a and b are different from those of Stuart. Donnelly and Simon[8] fitted several sets of torque measurements and found that $c \in \langle 1.33, 1.5 \rangle$.

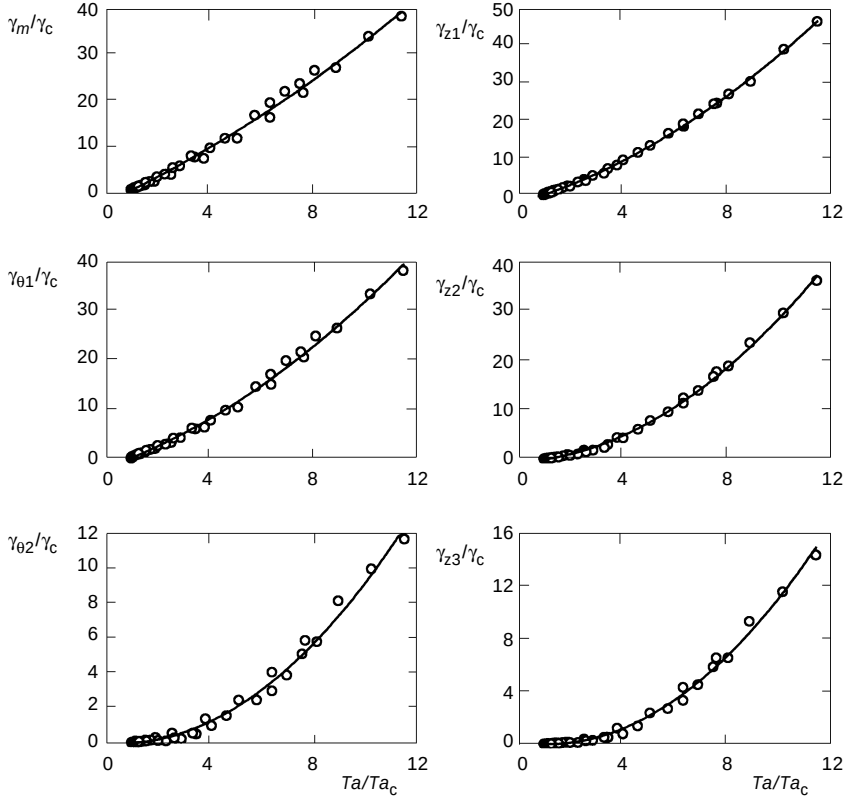

FIG. 11
Generalized dependence of Fourier coefficients, Eqs (*7*) and (*8*) on reduced Taylor number: ❍ experimental points, full lines – fit by second-order polynomials

Batchelor in an appendix to ref.[8] assumed that the vortex flow consists of inviscid cores surrounded by boundary layers and found that $c = 1.5$. Such a flow occurs at high Taylor numbers where the first term in Eq. (*11*) equals zero. The solutions of Stuart[15] and Davey[16] give coefficients a and b, but

TABLE II
Coefficients of polynomial fit $\gamma_{ik} = a_1(Ta/Ta_c)^2 + a_2(Ta/Ta_c) + a_3$

	a_1	a_2	a_3	$\Re$
γ_m	0.0850	2.6122	–1.7950	0.9944
$\gamma_{\theta 1}$	0.1484	1.9019	–1.7916	0.9964
$\gamma_{\theta 2}$	0.1054	–0.1081	–0.0045	0.9905
$\gamma_{\theta 3}$	0.0670	–0.2374	0.1869	0.9790
$\gamma_{\theta 4}$	0.0270	–0.1913	0.2246	0.9760
γ_{z1}	0.1955	2.0303	–1.9527	0.9993
γ_{z2}	0.2688	0.2561	0.6163	0.9983
γ_{z3}	0.1427	–0.3231	0.1712	0.9944
γ_{z4}	0.0714	–0.3689	0.3506	0.9870
γ_{z5}	0.0258	–0.1895	0.2247	0.9722

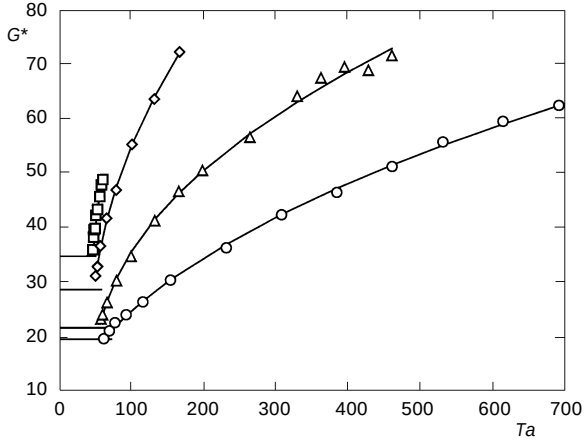

FIG. 12
Dependence of dimensionless torque on Taylor number, Eq. (*11*): ❐ $\eta = 0.8$, $a = -76\,500$, $b = 70.4$, $c = 0$; ✧ $\eta = 0.75$, $a = -26\,700$, $b = 6.90$, $c = 0.462$; Δ $\eta = 0.65$, $a = -23\,600$, $b = 5.43$, $c = 0.424$; ❍ $\eta = 0.6$, $a = -96.4$, $b = 2.78$, $c = 0.476$

they cannot be used to fit our experimental data with the exception of the Davey results valid not far beyond Ta_c. Therefore, our results for $\eta = 0.8$ were fitted by Eq. (*11*) with $c = 0$ and the results for $\eta = 0.75$, 0.65 and 0.6 by Eq. (*11*) with all terms. The full lines in Fig. 12 show these fits and the resulting values of *a*, *b* and *c* are given in the figure legend.

The wavelengths of vortices were calculated for each measurement and were found to be in the interval $\langle 2d, 2.4d \rangle$ (Table I). The axial velocity of vortices was about 10% higher than the mean axial velocity in the gap. The wavelengths of vortices were found to be smaller than $2d$ in our previous paper[10]. This was due to the unrealistic assumption that the vortices move with the mean axial velocity of the liquid.

CONCLUSIONS

Three-segment electrodiffusion probes are very convenient for measurements of the components of wall velocity gradients. The tangential and axial components of the wall velocity gradient at the outer wall of a Taylor–Couette flow with the inner cylinder rotating were mapped for four radius ratios, $\eta = 0.8$, 0.75, 0.65 and 0.6.

Jet-like flow was found at higher rotation rates. Stagnation lines of axial velocity occur at the outer wall where the jet impinges the wall, and separation lines where the liquid leaves the wall. As the flow is very stable, both lines are stable. The gradient of tangential velocity has a maximum value at the stagnation line and a minimum at the separation line.

The time histories of the velocity gradient components were described by fourth-order Fourier series. Generalized dependences were found of the Fourier series coefficients on the normalized Taylor number.

The axial velocity of vortices is about 10% higher than the mean velocity of the drifting flow.

The three-segment probes make it possible to calculate the torque from the mean value of the measured tangential component of the wall velocity gradient.

SYMBOLS

a, b, c	coefficients of Eq. (*11*)
a_1, a_2, a_3	coefficients of polynomial fit (Table II), s^{-1}
b_1, b_2, b_3	coefficients of Eq. (*3*), A $s^{1/3}$, A $s^{-1/3}$, A $s^{-1/6}$
c	concentration of depolarizer, mol m^{-3}
c_0	concentration of depolarizer in bulk, mol m^{-3}
D	coefficient of depolarizer diffusivity, m^2 s^{-1}

d	width of the gap between cylinders, m
F	Faraday constant, 96 485 C mol^{-1}
G	torque, N m
G^*	dimensionless torque, Eq. (*10*)
i	density of limiting diffusion current, A m^{-2}
I	limiting diffusion current, A
I_{tot}	total limiting diffusion current through segmented electrode, A
L	electrode length, m
n	number of electrons taking part in the electrochemical reaction
Pe	Peclet number, $Pe = \gamma L^2/D$
Re_{ax}	Reynolds number of axial flow, $Re_{ax} = \upsilon_{ax} d/\nu$
R_1, R_2	radii of inner and outer cylinders, m
$\Re$	correlation coefficient (Table II)
r, θ, z	cylindrical coordinates, m, rad, m
s	lag between currents of probes, s
Sc	Schmidt number, $Sc = \nu/D$
t	time, s
T	period of probe current, s
Ta	Taylor number, $Ta = \Omega R_1^{1/2} d^{3/2} \nu^{-1}$
υ	velocity, m s^{-1}
υ_{ax}	axial drifting velocity, m s^{-1}
U	voltage between working and auxiliary electrodes, V
W	electrode width, m
x, y	Cartesian coordinates, m
α	wavenumber, rad m^{-1}
δ	thickness of concentration boundary layer, m
ϕ	angle between reference radius of probe and flow direction, rad
φ_{ik}	phase in Eqs (*4*)–(*6*), rad
γ	magnitude of velocity gradient, $\gamma = (\gamma_\theta^2 + \gamma_z^2)^{1/2}$, s^{-1}
γ_θ	azimuthal component of velocity gradient at wall, Eq. (*7*), s^{-1}
γ_z	axial component of velocity gradient at wall, Eq. (*8*), s^{-1}
γ_m	mean value of azimuthal component of velocity gradient, Eq. (*7*), s^{-1}
γ_{ik}	harmonics of velocity gradient components, Eqs (*7*) and (*8*), s^{-1}
μ	dynamic viscosity, Pa s
ν	kinematic viscosity, m^2 s^{-1}
η	radius ratio, $\eta = R_1/R_2$
Ω	rotation rate of inner cylinder, rad s^{-1}

Subscripts

c	transition from laminar Couette flow to Taylor vortices
i	r, θ, z
k	ordinal of harmonics
r, θ, z	cylindrical coordinates
x, y	Cartesian coordinates

The author expresses his thanks to the Grant Agency of the Czech Republic which enabled this work by the grant No. 104/95/0654. This work was also partially supported by the European research project COST OC.F2.10 Electrochemical sensors for flow measurements. The poly(alkylene glycol) Emkarox HV 45 was donated by ICI, Frankfurt (Germany), and the resins Epoxy 521 and 1200 by the United Chemical and Metallurgical Works, Ltd., Ústí n. L. (Czech Republic). Many thanks are also expressed to Prof. G. Cognet, LEGI, Grenoble, France who initiated this project.

REFERENCES

1. Coles D: *J. Fluid Mech.* **1965**, *21*, 385.
2. Chossat P., Iooss G.: *The Couette–Taylor Problem*. Springer, New York 1994.
3. Donnelly R. J. in: *Ordered and Turbulent Patterns in Taylor–Couette Flow* (C. A. Andereck and F. Hayot, Eds), p. 1. Plenum Press, New York 1992.
4. Legrand J., Coeuret F.: *Chem. Eng. Sci.* **1986**, *41*, 47.
5. Desmet G., Verelst H., Baron G. V.: *Chem. Eng. Sci.* **1995**, *51*, 1299.
6. Kataoka K., Ohmura N., Kouzu M., Okubo M.: *Chem. Eng. Sci.* **1994**, *50*, 1409.
7. Mikulášek P.: *Collect. Czech. Chem. Commun.* **1994**, *59*, 737.
8. Donnelly R. J., Simon N. J.: *J. Fluid Mech.* **1960**, *7*, 401.
9. Cognet G.: *J. Mécanique* **1971**, *10*, 65.
10. Sobolík V., Benabes B., Cognet G.: *J. Appl. Electrochem.* **1995**, *25*, 441.
11. Selman J. R., Tobias C. W.: *Adv. Chem. Eng.* **1978**, *10*, 212.
12. Leveque M. A.: *Ann. Mines* **1928**, *13*, 201.
13. Sobolík V., Tihon J., Wein O., Wichterle K.: *J. Appl. Electrochem.* **1998**, *28*, 329.
14. Chandrasekhar S.: *Hydrodynamic and Hydromagnetic Stability*. Dover Publications, New York 1961.
15. Stuart J. T.: *J. Fluid Mech.* **1958**, *4*, 1.
16. Davey A.: *J. Fluid Mech.* **1962**, *14*, 336.
17. Di Prima R. C., Swinney H. L.: *Top. Appl. Phys.* **1981**, *45*, 139.
18. Wein O., Sobolík V.: *Collect. Czech. Chem. Commun.* **1989**, *54*, 3043.